ACS APPLIED MATERIALS & INTERFACES

Research Article

www.acsami.org

Highly Active Carbon Supported Pd–Ag Nanofacets Catalysts for Hydrogen Production from HCOOH

Wenhui Wang,[†,‡] Ting He,[†,‡] Xuehua Liu,[†] Weina He,[†] Hengjiang Cong,[§] Yangbin Shen,[†] Liuming Yan,[‡] Xuetong Zhang,[†] Jinping Zhang,[†] and Xiaochun Zhou*[,†,∥]

[†]Division of Advanced Nanomaterials, Suzhou Institute of Nano-tech and Nano-bionics, Chinese Academy of Sciences, Suzhou 215125, China

[‡]Department of Chemistry, College of Sciences, Shanghai University, 99 Shangda Road, Shanghai 200444, China

[§]College of Chemistry and Molecular Science, Wuhan University, Wuhan 430072, China

[∥]Key Laboratory of Nanodevices and Applications, Suzhou Institute of Nano-tech and Nano-bionics, Chinese Academy of Sciences, Suzhou 215125, China

S *Supporting Information*

ABSTRACT: Hydrogen is regarded as a future sustainable and clean energy carrier. Formic acid is a safe and sustainable hydrogen storage medium with many advantages, including high hydrogen content, nontoxicity, and low cost. In this work, a series of highly active catalysts for hydrogen production from formic acid are successfully synthesized by controllably depositing Pd onto Ag nanoplates with different Ag nanofacets, such as Ag{111}, Ag{100}, and the nanofacet on hexagonal close packing Ag crystal (Ag{hcp}). Then, the Pd–Ag nanoplate catalysts are supported on Vulcan XC-72 carbon black to prevent the aggregation of the catalysts. The research reveals that the high activity is attributed to the formation of Pd–Ag alloy nanofacets, such as Pd–Ag{111}, Pd–Ag{100}, and Pd–Ag{hcp}. The activity order of these Pd-decorated Ag nanofacets is Pd–Ag{hcp} > Pd–Ag{111} > Pd–Ag{100}. Particularly, the activity of Pd–Ag{hcp} is up to an extremely high value, i.e., $TOF_{\{hcp\}}$ = 19 000 ± 1630 h^{-1} at 90 °C (lower limit value), which is more than 800 times higher than our previous quasi-spherical Pd–Ag alloy nanocatalyst. The initial activity of Pd–Ag{hcp} even reaches (3.13 ± 0.19) × 10^6 h^{-1} at 90 °C. This research not only presents highly active catalysts for hydrogen generation but also shows that the facet on the hcp Ag crystal can act as a potentially highly active catalyst.

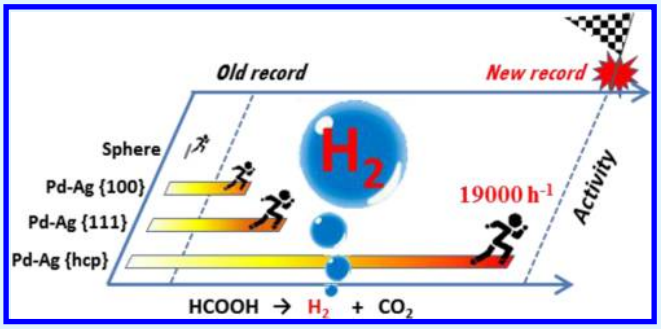

KEYWORDS: *hydrogen production, formic acid, Pd, nanofacet, hexagonal close packing*

1. INTRODUCTION

Hydrogen is regarded as a future sustainable and clean energy carrier.[1] However, the production and storage of hydrogen still have some challenging problems, such as low efficiency, high operating temperature, huge volume and weight loading, and excessive CO content. To solve these problems, formic acid (FA) is used, being an outstanding hydrogen storage medium with many advantages, including high hydrogen content (4.4 wt %), nontoxicity, and low cost.[2−7] To produce hydrogen from FA, it is necessary to dehydrogenate FA through[5]

$$HCOOH \rightarrow H_2 + CO_2 \quad \Delta G^{\ominus} = -48.4\ kJ\ mol^{-1} \qquad (1)$$

A catalyst is always needed to dehydrogenate FA at low temperatures (<100 °C). Thus, both homogeneous and heterogeneous catalysts for FA dehydrogenation have been successfully developed. The homogeneous catalysts are mainly some coordination compounds with metal cores such as ruthenium,[3,4] iridium,[8] and rhodium.[9] These homogeneous catalysts usually show very high catalytic activity.[10,11] On the other hand, heterogeneous catalysts are also studied alongside the homogeneous ones. The antipoisoning heterogeneous catalysts are usually Pd-based[5] or Au-based[12] nanocatalysts, which can continuously catalyze FA dehydrogenation to H_2 with trace or even without CO. Such hydrogen could be directly fed into a proton exchange fuel cell (PEMFC) to achieve high performance.[13,14]

Recently, researchers have made great achievements with regard to heterogeneous catalysts for the FA dehydrogenation reaction. First, special nanostructures, such as ultrafine palladium nanoparticles[15] and the core–shell structure,[16,17] were used in an attempt to improve the activity of Pd-based catalysts. Xu et al. found that ultrafine palladium nanoparticles with a small size and a clean surface have a high TOF, up to 7256 h^{-1} at 60 °C.[15] Tsang et al. found that the Pd shell

Received: July 4, 2016
Accepted: July 25, 2016
Published: July 25, 2016

DOI: 10.1021/acsami.6b08091
ACS Appl. Mater. Interfaces 2016, 8, 20839–20848

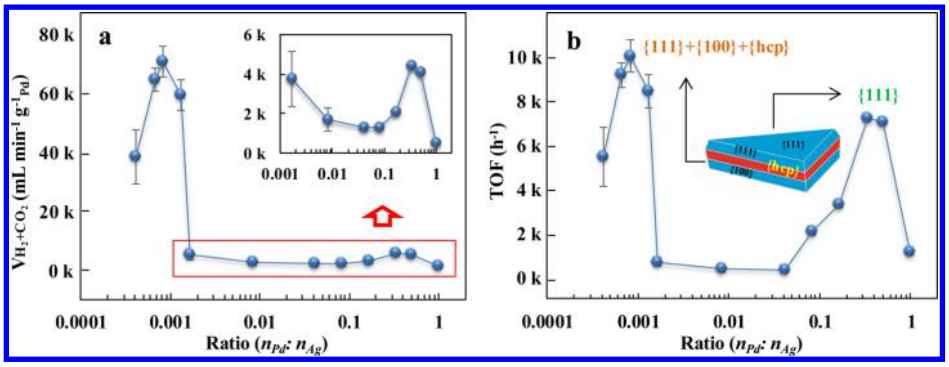

Figure 1. Activity of Pd–Ag nanoplate catalysts for FA dehydrogenation under steady state at 90 °C at different ratios of n_{Pd}:n_{Ag}, expressed in two ways. (a) Volume rate per Pd weight. (b) TOF. The catalyst at each ratio of n_{Pd}:n_{Ag} has 2–4 parallel samples; their average performances are presented in this figure. The volume is at the standard situation. TOF calculation is based on the Pd atoms on the nanoplate surface.

contains terrace sites and is electronically promoted by the Ag core, leading to significantly enhanced catalytic properties.[16]

Second, other metals or additives, such as Cu,[18] Ag,[5] Au,[13,19] Co,[20] Ni,[21] B,[22] MnO_x,[23] rare earth elements,[13] and Schiff base,[24] were added to Pd-based catalysts to improve the activity. These metals or additives usually have different functions in improving the activity. The addition of other metals, e.g., Cu,[18] Ag,[5] Au,[13,19] Co,[20] Ni,[21] and B,[22] could electronically promote Pd sites to significantly higher catalytic activity, as well as to a better tolerance toward CO poisoning via the synergetic effects between other metals and Pd.[5,13,18−22] The addition of metal oxide, e.g., MnO_x[23] and rare earth elements,[13] could provide sacrificial CO anchoring sites, forming carbonates. As a result, Pd-based active sites remain available for the dehydrogenation of FA for an extended duration. PdAu-MnO_x nanoparticles can produce hydrogen through additive-free FA dehydrogenation, with previously unprecedented activity (TOF = 785 mol H_2 mol catalyst^{-1} h^{-1} at room temperature).[25] Zhang et al. invented a Schiff base modified gold catalyst for efficient H_2 production from FA, with a TOF of 4368 h^{-1} at 50 °C.[24] The addition of a Schiff base could provide a synergetic effect for C–H activation between the protonated Schiff base and electronegative gold nanoparticles at the interface and increase the FA dehydrogenation.

Third, supports, such as ZIF-8-rGO,[26] nanoporous carbon MSC-30,[27] amine-functionalized SiO_2,[25] TiO_2,[28] reduced graphene oxide (RGO),[29] and macroreticular basic resin,[18,30] were also found to be very effective in improving the activity. These supports usually have very high specific surface area, which is advantageous in preparing well-dispersed ultrafine catalyst nanoparticles.[26,27] So far, very highly active Pd-based catalysts were achieved by using the Pd/MSC-30 catalyst (2623 h^{-1} at 50 °C)[27] and$(Co_6)Ag_{0.1}Pd_{0.9}$/RGO (2739 h^{-1} at 50 °C).[29] The supports can also have strong electron-donating effects on Pd and enhance the adsorption of formate to the catalyst and dehydrogenation from formate.[28] The supports with an amine functional group play a positive role in the O–H bond cleavage of FA.[18,25,30] A catalyst on basic resin showed a high reaction rate of more than 6000 mL min^{-1} g^{-1} (Pd), with a high TOF of 1900 h^{-1} based on Pd at 75 °C.[30]

However, the facet, one of the most important factors in heterogeneous catalysis,[31−34] has rarely been investigated in FA dehydrogenation.[35] It is well-known that different facets on a catalyst may yield different reaction activity and selectivity.[31,32] Recently, studies of different facets on a nanocrystal have attracted more and more attention in various catalytic reactions.[31,33,34,36−40] Some of the studies are focused on facets with monometal or metal oxide.[33,41] However, additional attention must be paid to facets with multimetals because such type of facets usually shows better activity and selectivity due to both a mediated electronic structure and surface atomic arrangement.[5,42,43] Therefore, it is possible to further improve the activity of a heterogeneous catalyst by modulating the facet on the catalyst for FA dehydrogenation.

Here, we report a series of highly active catalysts, which are synthesized by controllably depositing Pd onto different facets of Ag nanocrystals. Particularly, the activity of Pd-decorated facets on a hexagonal close packing Ag crystal (Ag{hcp}) reaches an extremely high value of 19 000 ± 1630 h^{-1} (turnover frequency (TOF)) at 90 °C, which is more than 800 times higher than that of the quasi-spherical Pd–Ag alloy nanocatalyst.

2. RESULTS AND DISCUSSION

2.1. Highly Active Catalysts with Pd-Decorated Ag Nanoplate for FA Dehydrogenation. To make the catalyst, Ag nanoplates with 88 ± 37 nm average edge length and 6.35 ± 1.00 nm average thickness (Figure S1) were prepared according to the literature.[44] The Pd-decorated Ag nanoplate catalysts with different n_{Pd}:n_{Ag} were synthesized by reducing different amounts of $PdCl_2$ with ascorbic acid onto an Ag nanoplate. Then, the nanoplate catalysts with multiple Pd–Ag nanofacets were supported on Vulcan XC-72 carbon black to prevent the aggregation of catalysts.

Notably, Figure 1 shows that the Pd–Ag nanoplate catalysts exhibit extremely high activity for FA dehydrogenation at 90 °C. Figure 1a,b also shows that there are two activity peaks of Pd–Ag nanoplate catalysts at n_{Pd}:n_{Ag} = 8.33 × 10^{-4} and 0.33. These two activity peaks are, incredibly, up to 64 300 ± 4870 mL min^{-1} g_{Pd}^{-1} (or 9170 ± 690 h^{-1}) at n_{Pd}:n_{Ag} = 8.33 × 10^{-4} and 4430 ± 40 mL min^{-1} g_{Pd}^{-1} (or 6570 ± 60 h^{-1}) at n_{Pd}:n_{Ag} = 0.33, respectively (lower limit value is used; see SI.17 for details). Both of them are much higher than our previous report for the quasi-spherical Pd–Ag alloy nanocatalyst (160 mL min^{-1} g_{Pd}^{-1} or TOF = 22 h^{-1} at 92 °C).[5]

2.2. Discover the Highly Active Locations on Pd-Decorated Ag Nanoplate Catalysts. Previous studies show that only one activity peak appears at the optimum Pd content (~50%) in the Pd–Ag alloy nanocatalyst for FA dehydrogenation.[5,16] Either a too high or a too low Pd content will cause lower catalytic activity of a Pd–Ag catalyst. However, this research shows that there are two activity peaks with the

DOI: 10.1021/acsami.6b08091
ACS Appl. Mater. Interfaces 2016, 8, 20839−20848

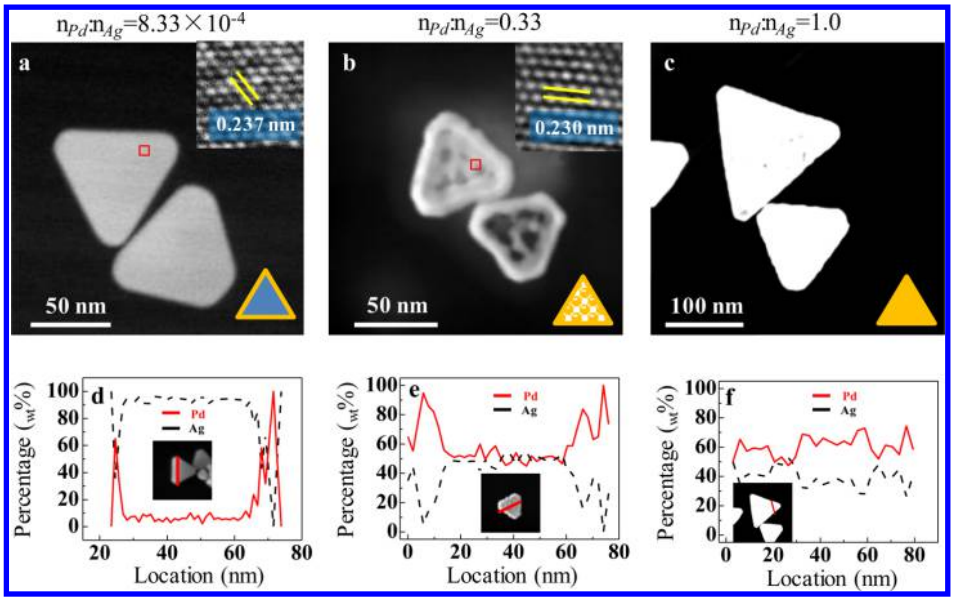

Figure 2. Controllably deposit Pd on different locations of Ag nanoplate by controlling the mole ratio of Pd to Ag (n_{Pd}:n_{Ag}). (a–c) HADDF-STEM images of Pd–Ag nanoplates at different n_{Pd}:n_{Ag}. (d–f) EDX measurement along the red line of the nanoplate in the inset at different n_{Pd}:n_{Ag}. (a, d) n_{Pd}:n_{Ag} = 8.33 × 10^{-4}; (b, e) n_{Pd}:n_{Ag} = 0.33; (c, f) n_{Pd}:n_{Ag} = 1.0. The insets in (a) and (b) show the HRTEM images of the corresponding Pd–Ag nanoplate. More images are found in Figure S2.

increase of Pd content in Figure 1. In this paper, because a Ag nanoplate has different facets, e.g., Ag{111} and Ag{100}, at different locations,[45] we could suppose that the two activity peaks in Figure 1 originate from different locations of the Ag nanoplate. In this section, by tracking the Pd content at different locations of the nanoplate, we try to determine the highly active locations on Pd-decorated Ag nanoplate catalysts.

Figure 2a shows that the shape and contrast of Pd-decorated Ag nanoplates at the low ratio n_{Pd}:n_{Ag} = 8.33 × 10^{-4} are similar to those of the as-synthesized Ag nanoplate in Figure S1. However, Figure 2d shows that the edges of the nanoplate have much higher Pd content compared to the mid part, indicating that most of the Pd deposits on the edges of the Ag nanoplate at a low ratio of n_{Pd}:n_{Ag}. Moreover, the edges can reach an optimum Pd content (~50%),[5,16,40] while the mid part has a too low Pd content to have high activity at this moment. Therefore, the first activity peak at the low ratio n_{Pd}:n_{Ag} = 8.33 × 10^{-4} should be attributed to the edges of the nanoplate.

At the high ratio of n_{Pd}:n_{Ag} = 0.33, Figure 2b shows that the edges of the Pd–Ag nanoplate are whiter and thicker relative to the mid part, indicating that more Pd prefers to deposit on the edges. The shape and size of the Ag nanoplate can be fixed at the beginning of the synthesis of the PdAg/C nanoplate catalyst. Hence, Figure 2b shows that there is a thin frame around the nanoplate. The EDX measurement in Figure 2e shows that the edges of the Ag nanoplate indeed have higher Pd content compared to the mid part. However, the Pd content on the edges could be up to 90%, which is too high to show high activity.[5] However, at such a ratio, the mid part has an optimum Pd content (~50%). Therefore, the second activity peak at the high ratio of 0.33 in Figure 1 should be attributed to the mid part of the nanoplate.[5,16,40]

At other ratios of n_{Pd}:n_{Ag}, neither the edges nor the mid part has an optimum Pd content (~50%) and the Pd–Ag nanoplate will show lower activity compared to the activity peaks. First, at a ratio n_{Pd}:n_{Ag} lower than 8.33 × 10^{-4}, the edges will have a Pd content lower than 50% and the mid part has a too low Pd content to have high activity. At such a condition, the activity decreases with decreasing ratio n_{Pd}:n_{Ag} in Figure 1. Second, at a ratio n_{Pd}:n_{Ag} higher than 8.33 × 10^{-4} but lower than 0.33, the edges will be covered by too much Pd and the mid part has a Pd content lower than 50%. Therefore, we could see a low ebb of activity in Figure 1 in the range of n_{Pd}:n_{Ag} between 8.33 × 10^{-4} and 0.33. Third, at a ratio n_{Pd}:n_{Ag} higher than 0.33, both the edges and the mid part have too much Pd and the Pd content is larger than 50% at every location on the entire nanoplate. For example, Figure 2f shows that both the edges and the mid part of the Pd–Ag nanoplate have an overhigh Pd content (>50%) at a high ratio of n_{Pd}:n_{Ag} = 1.0. Thus, the Pd–Ag nanoplate with a high ratio of n_{Pd}:n_{Ag} shows lower activity in Figure 1.

2.3. Identify the Nanofacets at the Highly Active Locations on the Pd–Ag Nanoplate Catalyst. The above research determined the exact locations on the Pd–Ag nanoplate catalyst for the two activity peaks in Figure 1. In this section, we will uncover why the edges and the mid part of the Pd–Ag nanoplate have such high activity compared to the quasi-spherical Pd–Ag alloy nanocatalyst. Both our experiment (Figure S3) and literature show that each individual Ag nanoplate has a three-layer structure.[45,46] These three layers include a defect-induced hcp Ag crystal layer, which is sandwiched between two face-centered cubic (fcc) layers (Figures S1 and S3). The triangular planes have a {111} facet, and the edges have three facets including {111}, {100}, and the facet on the hcp Ag crystal (abbreviated as {hcp}) (Figure 3a and Figure S3).[45] Therefore, the two activity peaks in Figure 1 are probably attributed to the different activities of different nanofacets on the triangular planes and the edges, respectively.

The first peak activity (9170 ± 690 h^{-1} at 90 °C) at the low ratio of n_{Pd}:n_{Ag} = 8.33 × 10^{-4} is probably attributed to the average activity of the three facets, including Pd–Ag{111}, Pd–Ag{100}, and Pd–Ag{hcp}, because most of the Pd is deposited on the edges. Figure 2a shows that the shape and contrast of the Pd–Ag nanoplate at a low ratio are almost the same as those of the as-synthesized Ag nanoplate in Figure S3.

DOI: 10.1021/acsami.6b08091
ACS Appl. Mater. Interfaces 2016, 8, 20839–20848

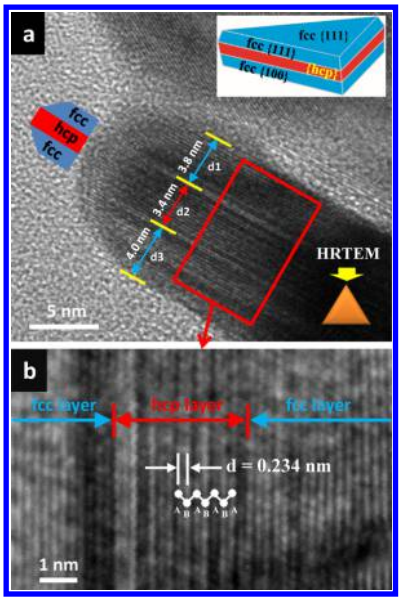

Figure 3. HRTEM image of a vertically oriented Pd–Ag nanoplate catalyst at n_{Pd}:n_{Ag} = 8.33 × 10^{-4}. (a) HRTEM image of the edge of a vertically oriented Pd–Ag nanoplate. The inset on the top right indicates that the hcp layer is sandwiched between two fcc layers. The inset on the bottom right indicates that the HRTEM measurement was taken parallel to the surface of the nanoplate. (b) Analysis of the structure within the area in (a). More images are found in Figure S4.

Moreover, Figure 3 shows that the fcc and hcp layers can survive at a low ratio of n_{Pd}:n_{Ag} = 8.33 × 10^{-4}. The hcp crystal structure can be clearly identified and measured in Figure 3b; the interface of hcp and fcc crystals is also clearly marked. Moreover, the area of the nanoplate edges cannot be omitted, although the Ag nanoplates in this paper have 88 ± 37 nm average edge length and 6.35 ± 1.00 nm average thickness. The total area of the edges is up to ~20% of the total area of the whole Ag nanoplate. Therefore, it is reasonable to assign the first peak activity at a low ratio of n_{Pd}:n_{Ag} to the average activity of the three facets, including Pd–Ag{111}, Pd–Ag{100}, and Pd–Ag{hcp}.

Note that there are many difficulties in taking an HRTEM image of a vertically oriented Ag or Pd–Ag nanoplate. First, it is difficult to make Ag or Pd–Ag nanoplates stand on their edges. Even if we increased the concentration of Ag or Pd–Ag nanoplates, only a low percentage of nanoplates will be vertically oriented on the copper grid for HRTEM measurement. Second, the Pd–Ag nanoplate should be in the right orientation during the HRTEM imaging. Otherwise, it is impossible to obtain a high-quality image with atom resolution. Third, it is difficult to obtain a high-quality image for both fcc and hcp crystals in one image because the orientations of fcc and hcp may be different in one nanoplate. Fourth, an hcp crystal is usually not perfect in an Ag or Pd–Ag nanoplate. There are possibly other defects at the interface between the fcc and hcp crystal or in the hcp crystal.[46] All the above difficulties make it extremely hard to obtain a high-quality image for a vertically oriented Ag or Pd–Ag nanoplate. Through several attempts, we overcame the difficulties and took some high-quality HRTEM images for both Ag and Pd–Ag nanoplates, as in the literature[45] (Figure 3, Figures S3 and S4).

The second peak activity (6570 ± 60 h^{-1} at 90 °C) at a high ratio of n_{Pd}:n_{Ag} = 0.33 should be attributed to the activity of the Pd–Ag{111} facet. From the previous section, we know that the second activity peak at a high ratio of 0.33 in Figure 1 should be attributed to the mid part of the nanoplate. The inset in Figure 2b clearly shows that the mid part is composed of a Pd–Ag{111} alloy facet because the lattice space is 0.230 nm, which is in the middle of Pd (0.220 nm) and Ag (0.240 nm).[47] The following XRD measurements also support this result.

2.4. Track the Variation of the Crystal Structure at Different n_{Pd}:n_{Ag}. To track the variation of the crystal structure with the increase of n_{Pd}:n_{Ag}, a series of XRD measurements were done. Figure 4a shows that the XRD pattern of the Ag nanoplate (black curve) has a strong {111} peak and other weaker peaks, i.e., {200}, {220}, and {311} of the fcc Ag metal (JCPDS file: 04-0783). In addition to the typical peaks of the fcc Ag crystal, there is a weak, but clear, peak that appears at 2θ ≈ 35.9° (black curve in Figure 4b), indicating the existence of the hcp Ag crystal structure in the Ag nanoplate. When the ratio of n_{Pd}:n_{Ag} is increased, the hcp crystal can survive at a low ratio of n_{Pd}:n_{Ag}, i.e., 8.33 × 10^{-4} (blue curve in Figure 4b), but will be totally destroyed at a high ratio of n_{Pd}:n_{Ag}, i.e., 0.33 (green curve in Figure 4b). This result

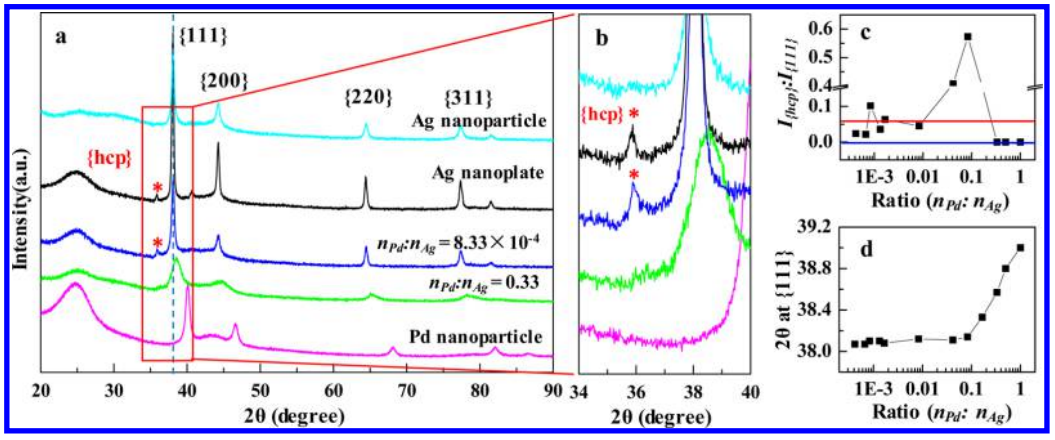

Figure 4. XRD measurements of Ag nanoparticles, Pd nanoparticles, Ag nanoplates, and Pd–Ag nanoplates with different molar ratios, i.e., n_{Pd}:n_{Ag} = 8.33 × 10^{-4} and 0.33. (a) XRD patterns (dashed line denotes standard {111} peak position of bulk Ag). (b) Magnification of (a) to uncover XRD peak for hcp structure. (c) The intensity ratios of hcp and {111} peaks ($I_{\{hcp\}}$:$I_{\{111\}}$) versus the different n_{Pd}:n_{Ag}. (d) The 2θ of Pd–Ag nanoplates catalysts on the {111} peak versus the different n_{Pd}:n_{Ag}. More images are found in Figure S6.

DOI: 10.1021/acsami.6b08091
ACS Appl. Mater. Interfaces 2016, 8, 20839–20848

is consistent with the observation of the HRTEM image in Figure 3 and Figure S4.

Figure 4c shows that the intensity ratios of {hcp} peak to {111} peak ($I_{\{hcp\}}$:$I_{\{111\}}$) remain at ~0.05 at n_{Pd}:n_{Ag} < 0.01, indicating that either the fcc or the hcp crystal structure of the Ag nanoplate does not have an obvious change at a low ratio (n_{Pd}:n_{Ag} < 0.01). With increasing n_{Pd}:n_{Ag}, $I_{\{hcp\}}$:$I_{\{111\}}$ increases and reaches a maximum value at the ratio of n_{Pd}:n_{Ag} = 0.083, indicating that the fcc crystal structure is destroyed much faster than that of the hcp. This may be because the hcp layer is protected by the two fcc crystal layers, which sandwich the two sides of the hcp layer. When n_{Pd}:n_{Ag} is higher than 0.33, the hcp crystal structure will be totally destroyed and the ratio $I_{\{hcp\}}$:$I_{\{111\}}$ will be zero in Figure 4c.

Figure 4a shows that 2θ at {111} for the Pd–Ag nanoplate only has a single peak at the location between the standard peaks of pure Ag ($2\theta_{\{111\}} \approx 38.1°$) and Pd ($2\theta_{\{111\}} \approx 40.1°$), indicating that a Pd–Ag alloy forms when Pd is deposited onto the Ag nanoplate. Thus, the high catalytic activity is due to the synergetic effect of Pd and Ag.[47] Moreover, Figure 4d shows that 2θ at {111} for the Pd–Ag nanoplate increases as the ratio of n_{Pd}:n_{Ag} increases. Interestingly, the curve in Figure 4d obviously has two parts, which are separated at n_{Pd}:n_{Ag} = ~0.1. This implies that the deposition of Pd on the triangular face (or body) of the Ag nanoplate dramatically happens from n_{Pd}:n_{Ag} = ~0.1. Therefore, it is supported again that the activity originates from the edges at low n_{Pd}:n_{Ag} but from the mid part at high n_{Pd}:n_{Ag}.

2.5. Activity of the Nanofacets Pd–Ag{111}, Pd–Ag{100}, and Pd–Ag{hcp}. Because the high activity ($TOF_{\{111\}+\{100\}+\{hcp\}}$ = 9170 ± 690 h^{-1} at 90 °C) is the average activity of three nanofacets, including Pd–Ag{111}, Pd–Ag{100}, and Pd–Ag{hcp}, we consider which one of them dominates the high activity. Currently, we know that the activity on the Pd–Ag{111} facet is $TOF_{\{111\}}$ = 6570 ± 60 h^{-1} at 90 °C, which is, however, much lower than $TOF_{\{111\}+\{100\}+\{hcp\}}$. Thus, the high activity should be mainly due to the Pd–Ag{100} or Pd–Ag{hcp} facet rather than the Pd–Ag{111} facet. However, it is difficult to directly synthesize the catalyst purely with the facet on the hcp Ag crystal due to the relative instability of the hcp Ag structure. However, it is much easier to synthesize the Pd–Ag nanowire catalyst mainly with the Pd–Ag{100} facet on its side wall.[48] If we can obtain the activity $TOF_{\{100\}}$ on the Pd–Ag{100} facet, then it is possible to know which one of the three facets is the most active one.

To obtain the activity of the Pd–Ag{100} nanofacet, we synthesized a series of Pd–Ag nanowire catalysts by depositing Pd onto the side wall of a silver nanowire through the same synthesis strategy as for the Pd–Ag nanoplate catalyst because the side wall of the Ag nanowire is composed of the {100} facet (Figure S8).[48] Figure S11 shows that the maximum activity ($TOF_{\{100\}}$ = 4080 ± 280 h^{-1} at 90 °C) of Pd–Ag nanowire catalysts appears at the ratio of n_{Pd}:n_{Ag} = 8.33 × 10^{-3}. However, it is also much lower than $TOF_{\{111\}+\{100\}+\{hcp\}}$. Thus, the Pd–Ag{hcp} facet plays a crucial role in the high catalytic activity of $TOF_{\{111\}+\{100\}+\{hcp\}}$ rather than the Pd–Ag{111} or Pd–Ag{100} facet.

To obtain the exact activity of Pd–Ag{hcp}, some calculations are required. Because $TOF_{\{111\}+\{100\}+\{hcp\}}$ is the average activity of the three facets

$$TOF_{\{111\}+\{100\}+\{hcp\}} = \alpha_1 TOF_{\{111\}} + \alpha_2 TOF_{\{100\}} + \alpha_3 TOF_{\{hcp\}} \quad (2)$$

$$\alpha_1 + \alpha_2 + \alpha_3 = 1 \quad (3)$$

where α_1, α_2, and α_3 are the fractions of the thicknesses of the two fcc crystal layers and one hcp crystal layer, respectively, which are calculated using $\alpha_1 = d_1/d$, $\alpha_2 = d_2/d$, $\alpha_3 = d_3/d$. The parameter d is the total thickness of the nanoplate, and d_1, d_2, and d_3 are the thicknesses of the two fcc crystal layers and one hcp crystal layer, respectively. The parameters d_1, d_2, and d_3 are also marked on the nanoplate in Figure 3a.

$$d = d_1 + d_2 + d_3 \quad (4)$$

Then, the activity of Pd–Ag{hcp} is

$$TOF_{\{hcp\}} = (TOF_{\{111\}+\{100\}+\{hcp\}} - \alpha_1 TOF_{\{111\}} - \alpha_2 TOF_{\{100\}})/\alpha_3 \quad (5)$$

According to our measurements (Figure S1) and the literature,[45] the thickness of the hcp layer (d_3) is 1.78 ± 0.50 nm and the thickness of the two fcc crystal layers (d_1, d_2, where $d_1 = d_2$) is 2.28 ± 0.25 nm. By using eq 5, we can determine the activity of Pd–Ag{hcp}, which is an extremely high value, i.e., $TOF_{\{hcp\}}$ = 19 000 ± 1630 h^{-1} at 90 °C. Therefore, Pd–Ag{hcp} dominates the high activity of $TOF_{\{111\}+\{100\}+\{hcp\}}$.

In this work, the activity of Pd–Ag{hcp} reaches 9790 h^{-1} at 60 °C and 19 000 h^{-1} at 90 °C, which is similar to the results in the literature, e.g., 7256 h^{-1} at 60 °C[15] and 2739 h^{-1} at 50 °C.[29] Therefore, this paper shows that the Pd-decorated Ag nanofacet is a type of highly active catalyst for the FA dehydrogenation reaction.

It is well-known that the hcp structure is not a natural crystal structure for metal silver and is less stable than the fcc structure. Thus, it is extremely difficult to study the catalyst made by the hcp Ag crystal. However, our work here shows that the catalyst with the hcp crystal can be synthesized by carefully controlling the synthesis conditions. The activity of the catalyst can reach a plate after 15 min (Figure S13).

2.6. Reaction Kinetics of FA Decomposition on Different Nanofacets. Why can these nanofacets show such high catalytic activity? The analysis of the reaction kinetics of FA decomposition on these facets may give us some answers. The FA decomposition on the Pd–Ag catalyst is a very complex reaction process, which mainly includes FA dehydrogenation, poisoning, and the refreshment process of the catalyst, as follows[13]

$$HCOOH + * \xrightarrow{k_1} * + H_2 + CO_2 \quad (6)$$

$$HCOOH + * \xrightarrow{k_2} * - CO + H_2O \quad (7)$$

$$* - CO \xrightarrow{k_3} * + CO \quad (8)$$

where k_1 is the FA dehydrogenation rate constant, k_2 is the poisoning rate constant, and k_3 is the refreshment rate constant. We adopt the model from our previous work[13] to describe the relationship between V and t:

DOI: 10.1021/acsami.6b08091
ACS Appl. Mater. Interfaces 2016, 8, 20839–20848

$$V = -\frac{k_1 k_2[\mathrm{HCOOH}]}{(k_2 + k_3)^2} e^{-(k_2+k_3)t} + \frac{k_1 k_3[\mathrm{HCOOH}]}{(k_2 + k_3)} t + \frac{k_1 k_2[\mathrm{HCOOH}]}{(k_2 + k_3)^2} + V_0 \quad (9)$$

Figure 5 shows that eq 9 can fit the experimental data of the facets Pd−Ag{111}, Pd−Ag{100}, and Pd−Ag{hcp} very well.

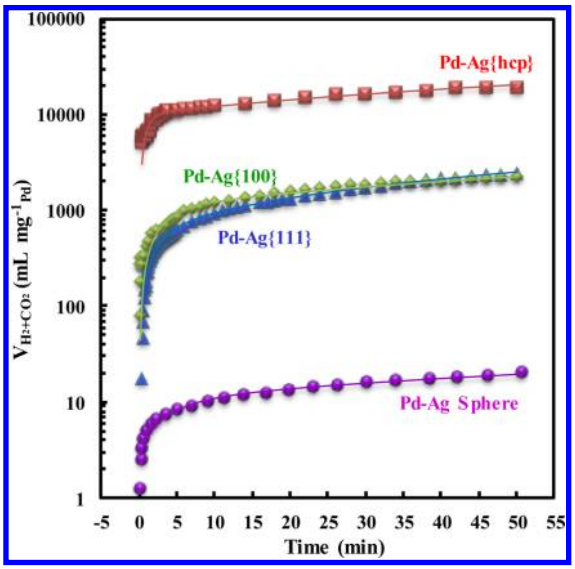

Figure 5. Kinetics analysis of FA decomposition on different nanofacets, including Pd−Ag{111}, Pd−Ag{100}, and Pd−Ag{hcp}. The experimental data (scattered symbols) for Pd−Ag{111}, Pd−Ag{100}, Pd−Ag{hcp}, and the sphere are from the Pd−Ag nanoplate at n_{Pd}:n_{Ag} = 0.33, Pd−Ag nanowire at n_{Pd}:n_{Ag} = 8.33 × 10^{-3} calculation (refer to the Experimental Section), and Pd−Ag spherical nanoparticle at n_{Pd}:n_{Ag} = 1, respectively. Refer to Figure S14 for the plot at the linear scale.

Through the fitting, the values of the parameters are obtained and listed in Table 1. From the fitting parameters, it can be

Table 1. Fitting Parameters for FA Decomposition Reaction on Different Surfaces[a]

Pd−Ag	k_1	k_2	k_3	k_1/k_2
sphere	1.65 ± 0.20	0.17 ± 0.02	0.0021 ± 0.0001	9.7
{111}	45.5 ± 0.9	0.28 ± 0.01	0.056 ± 0.002	163
{100}	66.9 ± 5.8	0.28 ± 0.04	0.022 ± 0.002	239
{hcp}	2190 ± 138	1.06 ± 0.09	0.020 ± 0.002	2070

[a]Unit of k_1: mL M^{-1} min^{-1} mg$_{Pd}^{-1}$; k_2: M^{-1} min^{-1} mg$_{Pd}^{-1}$; k_3: mL min^{-1} mg$_{Pd}^{-1}$.

calculated that the initial activity of Pd−Ag{hcp} can reach (3.13 ± 0.19) × 10^6 h^{-1} at 90 °C, while the initial activity of the Pd−Ag spherical nanoparticle is only 2350 ± 290 h^{-1} at 92 °C.

The model can also reflect the strength of certain chemical bonds or the ability of the catalyst in activating certain chemical bonds. Because the activation of the C−H bond is the rate-determining step of the FA dehydrogenation reaction in eq 6,[49,50] higher FA dehydrogenation rate constant k_1 reflects the higher ability of the catalyst in activating the C−H bond. For the facet Pd−Ag{hcp}, k_1 is up to 2190 ± 138 mL M^{-1} min^{-1} mg$_{Pd}^{-1}$, which is at least 30 times higher than that of other nanofacets. Thus, Pd−Ag{hcp} is extremely active in activating the C−H bond. This is one of the reasons for the high activity of the Pd−Ag{hcp} facet.

The poisoning step mainly relates to the breakage of C−H and C−OH bonds in eq 7. Because Pd−Ag{hcp} is extremely active in activating the C−H bond, the rate-determining step of the poisoning step should be the activation of the C−OH bond.[51] Hence, the poisoning rate constant k_2 mainly reflects the ability of the catalyst in activating the C−OH bond. Although k_2 of Pd−Ag{hcp} is also the maximum one compared to other facets, it is only ∼3 times higher than others. Thus, the poisoning step will not significantly affect the activity of the Pd−Ag{hcp} facet. Furthermore, the selectivity, i.e., k_1/k_2, of Pd−Ag{hcp} is up to 2070, which is also much higher than others.

The strength of the Pd−C bond determines the dissociation rate of CO_{ad} in eq 8. However, the refreshment rate constant k_3 of Pd−Ag{hcp} is similar to that of Pd−Ag{100}. Thus, the strength of the Pd−C bond on the Pd−Ag{hcp} facet is not so high and CO_{ad} can dissociate at a relatively high rate. More active surface will be exposed for catalysis through the refreshment process. This may be another reason for the high activity of the Pd−Ag{hcp} facet.

2.7. More Discussion about the Relationship between Activity and Nanofacets. Recently, the studies of different facets on a nanocrystal have attracted more and more attention in various catalytic reactions[31,33,34,36−40] because the crystal facet is one of the most important factors in the activity and selectivity in heterogeneous catalysis.[31−34] The atomic arrangement of the surface atoms can strongly affect the binding affinity of reactants, intermediates, and products during catalysis. If the atomic arrangement can match the geometry of adsorbed molecules, the adsorption will be strong. As we all know, either too weak or too strong binding of reactants will induce lower reaction activity.

Pd-based catalysts have high activities due to synergetic effects between Pd and other metals.[28,47,51] Pure Pd is active for formic acid decomposition, whereas pure Ag has no or only very weak activity. Previous studies showed that either a too high or a too low Pd content will cause lower catalytic activity of the Pd−Ag catalyst, and an activity peak will appear at the optimum Pd content (∼50%) in the Pd−Ag alloy nanocatalyst for FA dehydrogenation.[5,16] Moreover, other metals or additives, such as Cu,[18] Au,[13,19] Co,[20] Ni,[21] B,[22] MnO_x,[23] rare earth elements,[13] basic resin,[30] and Schiff base,[24] were added into Pd-based catalysts to improve the activity. However, Ag has not been found to have high activity when it is combined with other metals and additives. Thus, Pd atoms are the crucial element for the active sites in the Pd-based catalysts. The activity of a Pd-based active site is greatly improved when other metals and additives are involved. Some studies show that the drastic dehydrogenation activity enhancement is likely caused by their small size and the synergistic effect between Ag and Pd in the alloy structure, which inhibits the adsorption of CO on Pd.[47] The synergetic effects may be due to the electronic effect, which has been studied via X-ray photoelectron spectroscopy (XPS).[13] Then, the electronic structure, especially the d-band center position of the surface atoms, is modified.

In this paper, we controllably deposit Pd onto different facets of Ag nanocrystals to form Pd-based active sites. The synergetic effects between Pd and Ag clearly induce the activity peaks at different values of n_{Pd}:n_{Ag} in Figure 1. Figure S21a shows that the Pd 3d spectra of the Pd−Ag nanoplate catalyst (n_{Pd}:n_{Ag} = 0.33) could be fitted into four symmetric peaks, including the

DOI: 10.1021/acsami.6b08091
ACS Appl. Mater. Interfaces 2016, 8, 20839−20848

existence of two states of Pd species. The Pd $3d_{5/2}$ peak at 335.1 eV and Pd $3d_{3/2}$ peak at 340.4 eV are attributed to the metallic Pd(0), while the binding energy peaks shown at 335.7 and 341.0 eV are attributed to $3d_{5/2}$ and $3d_{3/2}$ of oxidic Pd(II). The higher peak area of Pd(0) indicates that the metallic state Pd is the dominant species on the surface of the Pd−Ag nanoplate catalyst (n_{Pd}:n_{Ag} = 0.33).[23] Figure S21b shows that the $3d_{5/2}$ and $3d_{3/2}$ peaks of Ag appear at 368.1 and 374.1 eV, indicating that most of the Ag will be in oxidic state Ag(I). Figure S21c,d shows that the catalyst has no chlorine element but has abundant oxygen element. Therefore, the oxidic state Ag(I) is possibly a type of silver oxide. Figure S21e shows the Pd 3d spectra of the Pd−Ag nanoplate catalyst (n_{Pd}:n_{Ag} = 8.33 × 10^{-4}). The content of Pd is so low that the XPS signal is noisy. Nevertheless, we can still identify the typical peaks for Pd 3d. Then, we tried to fit the Pd 3d spectra with four symmetric peaks. Figure S21f shows that the peak area of Pd(II) is much smaller than that of Pd(0), indicating that metallic Pd dominates on the surface of the Pd−Ag/C nanoplate catalyst (n_{Pd}:n_{Ag} = 8.33 × 10^{-4}). Figure S21f shows that the $3d_{5/2}$ and $3d_{3/2}$ peaks of Ag appear at 368.3 and 374.3 eV, indicating that most of the Ag is in metallic states.[52] Hence, the high activity of the Pd−Ag nanoplate catalyst is highly possibly due to the synergetic effect between the metallic state of Pd and Ag.[47]

The above discussion shows that the atomic arrangement of different facets and the electronic structure can affect the adsorption of molecules. Although this research cannot give the binding affinities of every species, Table 1 shows that the refreshment rate constant k_3 of Pd−Ag{hcp} is similar to that of Pd−Ag{100}, indicating that the strength of the Pd−C bond on the Pd−Ag{hcp} facet is similar to that of Pd−Ag{100}. Namely, the poisonous intermediate CO_{ad} has a comparable binding affinity on both the Pd−Ag{hcp} facet and Pd−Ag{100}. Therefore, the comparable binding affinity of CO_{ad} is one of the reasons for the extremely high activity of the Pd−Ag{hcp} facet.

As we all know, Pd and Ag classically have an fcc crystal. However, in this paper, the Pd−Ag alloy with an hcp crystal, i.e., Pd−Ag{hcp}, has been synthesized at room temperature because of the nanosize effect. Moreover, Pd−Ag{hcp} shows extremely high activity for formic acid dehydrogenation. This result indicates that the variation of crystal phase can strongly affect the catalytic activity of the nanocatalyst. There is rising interests in crystal phase-controlled synthesis, properties, and applications of noble metal nanomaterials.[53−55] For example, the 4H/fcc Au@PdAg nanoribbons exhibit much higher electrocatalytic activity toward the hydrogen evolution reaction compared to that of Pd black, which is even quite close to that of the commercial Pt black.[54] Therefore, this research again shows that the activity and selectivity can be greatly modified by finely controlling the crystal phase of the nanocatalyst.

3. CONCLUSION

Pd was successfully deposited onto different nanofacets of triangular-shaped Ag nanocrystals. Vulcan XC-72 carbon black was used to prevent the aggregation of Pd−Ag nanofacets catalysts. The Pd-decorated Ag nanofacets exhibit very high activity in FA dehydrogenation, with an order Pd−Ag{hcp} > Pd−Ag{111} > Pd−Ag{100} at the optimum Pd content (~50%). Particularly, the activity of Pd−Ag{hcp} is up to an extremely high value, i.e., $TOF_{\{hcp\}}$ = 19 000 ± 1630 h^{-1} at 90 °C, which is much higher than the activity of other Pd-based catalysts. The initial activity of Pd−Ag{hcp} even reaches (3.13 ± 0.19) × 10^6 h^{-1} at 90 °C. This research not only presents highly active catalysts for hydrogen generation but also shows that the nanofacet on the hcp Ag crystal is a potentially highly active catalyst.

4. EXPERIMENTAL SECTION

4.1. Materials and Characterizations. All commercial materials were used as received unless specified. All aqueous solutions were prepared using deionized water in air. X-ray diffraction (XRD) patterns for the catalysts were recorded using a Bruker D8 X-ray diffractometer with the Cu−Kα (λ = 1.5406 Å) radiation source operating at 40 kV and 40 mA. The nanostructure and composition of silver nanoplates, Ag nanowires, and Pd−Ag catalysts were characterized by TEM, high-resolution TEM (HRTEM), high-angle annular dark-field scanning transmission electron microscopy, (HADDF-STEM) and EDX (EDAS) (200 kV, Tecnai G2 F20 S-TWIN; FEI) at CAS-Platform for Characterization & Test in the Suzhou Institute of Nanotech and Nanobionics.

4.2. Synthesis of Ag Nanoplates. In a typical synthesis of silver nanoplates,[44] an aqueous solution of silver nitrate (Aladdin, 99.8%) (0.1 M, 4 mL) and trisodium citrate (Sinopharm Chemical Reagent Co., Ltd.) (75 mM, 80 mL) were added into 1920 mL of pure water with vigorous stirring at room temperature. Then, sodium borohydride (Sinopharm Chemical Reagent Co., Ltd., 96%) ($NaBH_4$, 0.1 M, 40 mL) was rapidly injected into the mixture, followed by injecting H_2O_2 (Sinopharm Chemical Reagent Co., Ltd.) (30 wt %, 14 mL) drop by drop. In the next several minutes, the solution color changed from yellow to blue, indicating that the morphology changed from sphere to nanoplate. The resulting solution was kept stirring for 4 h at room temperature.

4.3. Synthesis of Ag Nanowires. Silver nanowires were synthesized by the method presented by Xia et al.[56] Typically, 0.1 mol of NaCl (Enox, China) and 2.24 g of poly(vinyl pyrrolidone) (PVP, MW = 1 300 000) (Aldrich) were added to ethylene glycol (EG) (Sinopharm Chemical Reagent Co., Ltd.) and heated to obtain a clear solution. $AgNO_3$ solution (0.1 M, in EG) was added drop by drop to the solution with vigorous stirring for 10 min. The mixed solution was poured into a Teflon-lined stainless-steel autoclave, and was heated at 160 °C for 6 h. The product was diluted with ethanol (Sinopharm Chemical Reagent Co., Ltd.) or water and centrifuged at 4000 rpm for 5 min several times to remove the surfactant. Finally, the purified nanowires were dispersed in water. The as-synthesized Ag nanowires with 50.1 ± 8.5 nm diameter and 6.3 ± 3.6 μm length were characterized by TEM, SEM, and optical dark-field microscopy.

4.4. Synthesis of Pd−Ag Nanoplate and Nanowire Catalysts. First, ascorbic acid (Amresco) (AA, 65 mM, 5 mL) as the reductant and 10 mM $PdCl_2$ (Nanjing Precious Metal Factory, China) as the Pd source were successively injected into 340 mL of Ag nanoplates solution, which was heating at 40 °C in an oil bath for 2 h. The amount of Ag nanoplates was kept constant in the solutions while the amount of $PdCl_2$ was varied to achieve the different molar ratios of Pd to Ag (n_{Pd}:n_{Ag}) from 4.17 × 10^{-4} to 1.0. Subsequently, the resulting solution was poured into 200 mL of the suspension ($V_{ethanol}$:V_{water} = 1:1) with 100 mg of Vulcan XC-72 carbon black (Cabot Co.). The Pd−Ag nanoplates were spaced by the carbon black to prevent aggregating. Finally, the suspension was filtered and washed with distilled water, and then dried in oven at 80 °C overnight. The Pd−Ag nanowire catalysts were prepared with different molar ratios of n_{Pd}:n_{Ag} by using the same method as above.

4.5. Measurement of HCOOH Dehydrogenation Reaction. To measure the HCOOH (Sinopharm Chemical Reagent Co., Ltd., 98%) dehydrogenation reaction, 30 mg of catalyst was added into 5 mL of solution with 5 M formic acid and 2.5 M sodium formate. The reaction temperature was controlled at 90 °C by a thermostat bath. The product gas was collected by a 100 mL injector, and was monitored by a camera.

4.6. Calculation of Catalytic Activity. This paper will mainly focus on the catalytic activity for the steady state after reaction for 10 min. The catalytic activity was calculated through two ways, including

DOI: 10.1021/acsami.6b08091
ACS Appl. Mater. Interfaces 2016, 8, 20839−20848

the volume rate per Pd weight ($V_{CO_2+H_2}$, mL min^{-1} g_{Pd}^{-1}) and turnover frequency (TOF, h^{-1}). The volume is at the standard situation. The $V_{CO_2+H_2}$ was calculated by dividing the volume rate by the total weight of Pd in the reactor. The volume rate was calculated by dividing volume by the corresponding time. TOF was calculated according to the literature[13]

$$\text{TOF} = (\text{number of produced hydrogen molecules}) / (\text{reaction time} \times \text{number of Pd atoms on the surface}) \quad (10)$$

In the above equation, the number of produced hydrogen molecules and reaction time are easy to be obtained from experiment. However, the number of Pd atoms on the surface needs to be specifically calculated for different cases. On the basis of the TEM research, we found that Pd prefers depositing onto the edges of the Ag nanoplate at low ratio n_{Pd}:n_{Ag} (<0.0417), while homogeneously covering the entire surface of the Ag nanoplate at high ratio n_{Pd}:n_{Ag} (>0.0417). For the Ag nanowire, Figure S8 shows that Pd homogeneously covers the side wall of Ag nanowire according to TEM research. In addition, Pd−Ag alloy is formed on the nanoplates according to XRD research. Then, the number of Pd on the surface is calculated accordingly. Please refer to the Supporting Information (SI.17) for more detailed information.

4.7. Reaction Kinetics of FA Decomposition on Different Nanofacets. The reaction kinetics of FA decomposition on different facets was carried out according to the literature.[13] Some interesting kinetics parameters could be obtained by fitting the gas volume to time (V−t) curves for different nanofacets by the kinetics model in the literature.[13]

In order to do the kinetics analysis, it is necessary to obtain V−t curves for different nanofacets first. From experiment, we could directly obtain the V−t curves for Pd−Ag{111} and Pd−Ag{100} from the Pd−Ag nanoplate at n_{Pd}:n_{Ag} = 0.33 and the Pd−Ag nanowire at n_{Pd}:n_{Ag} = 8.33 × 10^{-3}, respectively. However, we need to do some calculations to obtain the V−t curve for Pd−Ag{hcp}.

From experiment, we could obtain the V−t curve for the edge of the Pd−Ag nanoplate, which includes the facets Pd−Ag{111}, Pd−Ag{100}, and Pd−Ag{hcp}. Therefore

$$V(t)_{\{111\}+\{100\}+\{hcp\}} = \alpha_1 V(t)_{\{111\}} + \alpha_2 V(t)_{\{100\}} + \alpha_3 V(t)_{\{hcp\}} \quad (11)$$

where $V(t)_{\{111\}}$, $V(t)_{\{100\}}$, $V(t)_{\{hcp\}}$, and $V(t)_{\{111\}+\{100\}+\{hcp\}}$ are the gas volume generated by Pd−Ag{111}, Pd−Ag{100}, Pd−Ag{hcp}, and Pd−Ag{111} + Pd−Ag{100} + Pd−Ag{hcp}, respectively, at the time t. Then

$$V(t)_{\{hcp\}} = (V(t)_{\{111\}+\{100\}+\{hcp\}} - \alpha_1 V(t)_{\{111\}} - \alpha_2 V(t)_{\{100\}}) / \alpha_3 \quad (12)$$

By the above equation, $V(t)_{\{hcp\}}$ could be calculated, since $V(t)_{\{111\}}$, $V(t)_{\{100\}}$, and $V(t)_{\{111\}+\{100\}+\{hcp\}}$ are already known. Then, the kinetics model in the literature was used to fit the V−t curves for different nanofacets to obtain some interesting kinetics parameters.[13] These parameters could help us understand the mechanism of the catalysis.

■ ASSOCIATED CONTENT

Supporting Information

The Supporting Information is available free of charge on the ACS Publications website at DOI: 10.1021/acsami.6b08091.

Experimental details and additional results (PDF)

■ AUTHOR INFORMATION

Corresponding Author

*E-mail: xczhou2013@sinano.ac.cn.

Notes

The authors declare no competing financial interest.

■ ACKNOWLEDGMENTS

The authors are grateful for financial support granted by Ministry of Science and Technology of China (No. 2016YFA0200700), the National Natural Science Foundation of China (No. 21373264, No. 21573275, No. 21210004), the Natural Science Foundation of Jiangsu Province (BK20150362), the Suzhou Institute of Nanotech and Nanobionics (Y3AAA11004), and the Thousand Youth Talents Plan (Y3BQA11001).

■ REFERENCES

(1) Park, S.; Vohs, J. M.; Gorte, R. J. Direct Oxidation of Hydrocarbons in A Solid-Oxide Fuel Cell. *Nature* **2000**, *404*, 265−267.

(2) Yadav, M.; Xu, Q. Liquid-Phase Chemical Hydrogen Storage Materials. *Energy Environ. Sci.* **2012**, *5*, 9698−9725.

(3) Guerriero, A.; Bricout, H.; Sordakis, K.; Peruzzini, M.; Monflier, E.; Hapiot, F.; Laurenczy, G.; Gonsalvi, L. Hydrogen Production by Selective Dehydrogenation of HCOOH Catalyzed by Ru-Biaryl Sulfonated Phosphines in Aqueous Solution. *ACS Catal.* **2014**, *4*, 3002−3012.

(4) Boddien, A.; Loges, B.; Junge, H.; Gärtner, F.; Noyes, J. R.; Beller, M. Continuous Hydrogen Generation from Formic Acid: Highly Active and Stable Ruthenium Catalysts. *Adv. Synth. Catal.* **2009**, *351*, 2517−2520.

(5) Zhou, X.; Huang, Y.; Xing, W.; Liu, C.; Liao, J.; Lu, T. High-Quality Hydrogen from the Catalyzed Decomposition of Formic Acid by Pd-Au/C and Pd-Ag/C. *Chem. Commun.* **2008**, 3540−3542.

(6) Johnson, T. C.; Morris, D. J.; Wills, M. Hydrogen Generation from Formic Acid and Alcohols using Homogeneous Catalysts. *Chem. Soc. Rev.* **2010**, *39*, 81−88.

(7) Li, F.-F.; Gu, J.-N.; Zhou, X.-C. Single Molecule Electro-Catalysis of Non-Fluorescent Molecule. *Chin. Chem. Lett.* **2015**, *26*, 1514−1517.

(8) Hull, J. F.; Himeda, Y.; Wang, W.-H.; Hashiguchi, B.; Periana, R.; Szalda, D. J.; Muckerman, J. T.; Fujita, E. Reversible Hydrogen Storage Using CO_2 and A Proton-Switchable Iridium Catalyst in Aqueous Media under Mild Temperatures and Pressures. *Nat. Chem.* **2012**, *4*, 383−388.

(9) Fukuzumi, S.; Kobayashi, T.; Suenobu, T. Efficient Catalytic Decomposition of Formic Acid for The Selective Generation of H2 and H/D Exchange with a Water-Soluble Rhodium Complex in Aqueous Solution. *ChemSusChem* **2008**, *1*, 827−834.

(10) Bielinski, E. A.; Lagaditis, P. O.; Zhang, Y.; Mercado, B. Q.; Würtele, C.; Bernskoetter, W. H.; Hazari, N.; Schneider, S. Lewis Acid-Assisted Formic Acid Dehydrogenation using A Pincer-Supported Iron Catalyst. *J. Am. Chem. Soc.* **2014**, *136*, 10234−10237.

(11) Wang, Z.; Lu, S.-M.; Li, J.; Wang, J.; Li, C. Unprecedentedly High Formic Acid Dehydrogenation Activity on An Iridium Complex with an *N*,*N*′-Diimine Ligand In Water. *Chem.—Eur. J.* **2015**, *21*, 12592−12595.

(12) Ojeda, M.; Iglesia, E. Formic Acid Dehydrogenation on Au-Based Catalysts at Near-Ambient Temperatures. *Angew. Chem., Int. Ed.* **2009**, *48*, 4800−4803.

(13) Zhou, X.; Huang, Y.; Liu, C.; Liao, J.; Lu, T.; Xing, W. Available Hydrogen from Formic Acid Decomposed by Rare Earth Elements Promoted Pd-Au/C Catalysts at Low Temperature. *ChemSusChem* **2010**, *3*, 1379−1382.

(14) Boddien, A.; Loges, B.; Junge, H.; Beller, M. Hydrogen Generation at Ambient Conditions: Application in Fuel Cells. *ChemSusChem* **2008**, *1*, 751−758.

(15) Zhu, Q.-L.; Tsumori, N.; Xu, Q. Immobilizing Extremely Catalytically Active Palladium Nanoparticles to Carbon Nanospheres: A Weakly-Capping Growth Approach. *J. Am. Chem. Soc.* **2015**, *137*, 11743−11748.

(16) Tedsree, K.; Li, T.; Jones, S.; Chan, C. W. A.; Yu, K. M. K.; Bagot, P. A. J.; Marquis, E. A.; Smith, G. D. W.; Tsang, S. C. E. Hydrogen Production from Formic Acid Decomposition at Room

DOI: 10.1021/acsami.6b08091
ACS Appl. Mater. Interfaces 2016, 8, 20839−20848

Temperature Using a Ag-Pd Core-Shell Nanocatalyst. *Nat. Nanotechnol.* **2011**, *6*, 302−307.
(17) Huang, Y.; Zhou, X.; Yin, M.; Liu, C.; Xing, W. Novel PdAu@Au/C Core−Shell Catalyst: Superior Activity and Selectivity in Formic Acid Decomposition for Hydrogen Generation. *Chem. Mater.* **2010**, *22*, 5122−5128.
(18) Mori, K.; Tanaka, H.; Dojo, M.; Yoshizawa, K.; Yamashita, H. Synergic Catalysis of PdCu Alloy Nanoparticles within a Macroreticular Basic Resin for Hydrogen Production from Formic Acid. *Chem.—Eur. J.* **2015**, *21*, 12085−12092.
(19) Metin, O.; Sun, X.; Sun, S. Monodisperse Gold-Palladium Alloy Nanoparticles and Their Composition-Controlled Catalysis in Formic Acid Dehydrogenation under Mild Conditions. *Nanoscale* **2013**, *5*, 910−912.
(20) Wang, Z.-L.; Yan, J.-M.; Ping, Y.; Wang, H.-L.; Zheng, W.-T.; Jiang, Q. An Efficient CoAuPd/C Catalyst for Hydrogen Generation from Formic Acid at Room Temperature. *Angew. Chem., Int. Ed.* **2013**, *52*, 4406−4409.
(21) Yurderi, M.; Bulut, A.; Zahmakiran, M.; Kaya, M. Carbon Supported Trimetallic PdNiAg Nanoparticles as Highly Active, Selective and Reusable Catalyst in The Formic Acid Decomposition. *Appl. Catal., B* **2014**, *160−161*, 514−524.
(22) Jiang, K.; Xu, K.; Zou, S.; Cai, W.-B. B-Doped Pd Catalyst: Boosting Room-Temperature Hydrogen Production from Formic Acid-Formate Solutions. *J. Am. Chem. Soc.* **2014**, *136*, 4861−4864.
(23) Bulut, A.; Yurderi, M.; Karatas, Y.; Say, Z.; Kivrak, H.; Kaya, M.; Gulcan, M.; Ozensoy, E.; Zahmakiran, M. MnOx-Promoted PdAg Alloy Nanoparticles for the Additive-Free Dehydrogenation of Formic Acid at Room Temperature. *ACS Catal.* **2015**, *5*, 6099−6110.
(24) Liu, Q.; Yang, X.; Huang, Y.; Xu, S.; Su, X.; Pan, X.; Xu, J.; Wang, A.; Liang, C.; Wang, X.; Zhang, T. A Schiff Base Modified Gold Catalyst for Green and Efficient H_2 Production from Formic Acid. *Energy Environ. Sci.* **2015**, *8*, 3204−3207.
(25) Karatas, Y.; Bulut, A.; Yurderi, M.; Ertas, I. E.; Alal, O.; Gulcan, M.; Celebi, M.; Kivrak, H.; Kaya, M.; Zahmakiran, M. Pdau-Mnox Nanoparticles Supported On Amine-Functionalized SiO_2 for the Room Temperature Dehydrogenation of Formic Acid in the Absence of Additives. *Appl. Catal., B* **2016**, *180*, 586−595.
(26) Yan, J.-M.; Wang, Z.-L.; Gu, L.; Li, S.-J.; Wang, H.-L.; Zheng, W.-T.; Jiang, Q. AuPd-MnOx/MOF-Graphene: an Efficient Catalyst for Hydrogen Production from Formic Acid at Room Temperature. *Adv. Energy Mater.* **2015**, *5*, 1500107−1500107.
(27) Zhu, Q.-L.; Tsumori, N.; Xu, Q. Sodium Hydroxide-Assisted Growth of Uniform Pd Nanoparticles on Nanoporous Carbon MSC-30 for Efficient and Complete Dehydrogenation of Formic Acid under Ambient Conditions. *Chem. Sci.* **2014**, *5*, 195−199.
(28) Hattori, M.; Einaga, H.; Daio, T.; Tsuji, M. Efficient Hydrogen Production from Formic Acid Using TiO_2-Supported AgPd@Pd Nanocatalysts. *J. Mater. Chem. A* **2015**, *3*, 4453−4461.
(29) Chen, Y.; Zhu, Q.-L.; Tsumori, N.; Xu, Q. Immobilizing Highly Catalytically Active Noble Metal Nanoparticles on Reduced Graphene Oxide: A Non-Noble Metal Sacrificial Approach. *J. Am. Chem. Soc.* **2015**, *137*, 106−109.
(30) Mori, K.; Dojo, M.; Yamashita, H. Pd and Pd−Ag Nanoparticles within a Macroreticular Basic Resin: an Efficient Catalyst for Hydrogen Production from Formic Acid Decomposition. *ACS Catal.* **2013**, *3*, 1114−1119.
(31) Gu, J.; Zhang, Y.-W.; Tao, F. F. Shape Control of Bimetallic Nanocatalysts through Well-Designed Colloidal Chemistry Approaches. *Chem. Soc. Rev.* **2012**, *41*, 8050−8065.
(32) Xu, L.; Luo, Z.; Fan, Z.; Zhang, X.; Tan, C.; Li, H.; Zhang, H.; Xue, C. Triangular Ag-Pd Alloy Nanoprisms: Rational Synthesis with High-Efficiency for Electrocatalytic Oxygen Reduction. *Nanoscale* **2014**, *6*, 11738−11743.
(33) Hua, Q.; Cao, T.; Gu, X.-K.; Lu, J.; Jiang, Z.; Pan, X.; Luo, L.; Li, W.-X.; Huang, W. Crystal-Plane-Controlled Selectivity of Cu_2O Catalysts in Propylene Oxidation with Molecular Oxygen. *Angew. Chem., Int. Ed.* **2014**, *53*, 4856−4861.
(34) Zhang, H.; Jin, M.; Wang, J.; Li, W.; Camargo, P. H. C.; Kim, M. J.; Yang, D.; Xie, Z.; Xia, Y. Synthesis of Pd-Pt Bimetallic Nanocrystals with A Concave Structure through A Bromide-Induced Galvanic Replacement Reaction. *J. Am. Chem. Soc.* **2011**, *133*, 6078−6089.
(35) Yu, W.-Y.; Mullen, G. M.; Flaherty, D. W.; Mullins, C. B. Selective Hydrogen Production from Formic Acid Decomposition on Pd-Au Bimetallic Surfaces. *J. Am. Chem. Soc.* **2014**, *136*, 11070−11078.
(36) Lim, B.; Jiang, M.; Camargo, P. H. C.; Cho, E. C.; Tao, J.; Lu, X.; Zhu, Y.; Xia, Y. Pd-Pt Bimetallic Nanodendrites with High Activity for Oxygen Reduction. *Science* **2009**, *324*, 1302−1305.
(37) Porter, N. S.; Wu, H.; Quan, Z.; Fang, J. Shape-Control and Electrocatalytic Activity-Enhancement of Pt-Based Bimetallic Nanocrystals. *Acc. Chem. Res.* **2013**, *46*, 1867−1877.
(38) Huang, X.; Tang, S.; Zhang, H.; Zhou, Z.; Zheng, N. Controlled Formation of Concave Tetrahedral Trigonal Bipyramidal Palladium Nanocrystals. *J. Am. Chem. Soc.* **2009**, *131*, 13916−13917.
(39) Chen, C.; Kang, Y.; Huo, Z.; Zhu, Z.; Huang, W.; Xin, H. L.; Snyder, J. D.; Li, D.; Herron, J. A.; Mavrikakis, M.; Chi, M.; More, K. L.; Li, Y.; Markovic, N. M.; Somorjai, G. A.; Yang, P.; Stamenkovic, V. R. Highly Crystalline Multimetallic Nanoframes with Three-Dimensional Electrocatalytic Surfaces. *Science* **2014**, *343*, 1339−1343.
(40) Zhou, K.; Li, Y. Catalysis Based on Nanocrystals with Well-Defined Facets. *Angew. Chem., Int. Ed.* **2012**, *51*, 602−613.
(41) Zhang, J.; Liu, P.; Lu, Z.; Xu, G.; Wang, X.; Qian, L.; Wang, H.; Zhang, E.; Xi, J.; Ji, Z. One-step Synthesis of Rutile Nano-TiO_2 with Wxposed {111} Facets for High Photocatalytic Activity. *J. Alloys Compd.* **2015**, *632*, 133−139.
(42) Watanabe, M.; Uchida, M.; Motoo, S. Preparation of Highly Dispersed Pt+Ru Alloy Clusters and the Activity for the Electrooxidation of Methanol. *J. Electroanal. Chem. Interfacial Electrochem.* **1987**, *229*, 395−406.
(43) Chen, Y.-X.; Chen, S.-P.; Zhou, Z.-Y.; Tian, N.; Jiang, Y.-X.; Sun, S.-G.; Ding, Y.; Wang, Z. L. Tuning the Shape and Catalytic Activity of Fe Nanocrystals from Rhombic Dodecahedra and Tetragonal Bipyramids to Cubes by Electrochemistry. *J. Am. Chem. Soc.* **2009**, *131*, 10860−10862.
(44) Zhang, Q.; Li, N.; Goebl, J.; Lu, Z.; Yin, Y. A Systematic Study of the Synthesis of Silver Nanoplates: Is Citrate A "Magic" Reagent? *J. Am. Chem. Soc.* **2011**, *133*, 18931−18939.
(45) Aherne, D.; Ledwith, D. M.; Gara, M.; Kelly, J. M. Optical Properties and Growth Aspects of Silver Nanoprisms Produced by A Highly Reproducible and Rapid Synthesis at Room Temperature. *Adv. Funct. Mater.* **2008**, *18*, 2005−2016.
(46) Bansal, V.; Li, V.; O'Mullane, A. P.; Bhargava, S. K. Shape Dependent Electrocatalytic Behaviour of Silver Nanoparticles. *CrystEngComm* **2010**, *12*, 4280−4286.
(47) Zhang, S.; Metin, O.; Su, D.; Sun, S. Monodisperse AgPd Alloy Nanoparticles and Their Superior Catalysis for the Dehydrogenation of Formic Acid. *Angew. Chem., Int. Ed.* **2013**, *52*, 3681−3684.
(48) Sun, Y.; Mayers, B.; Herricks, T.; Xia, Y. Polyol Synthesis of Uniform Silver Nanowires: A Plausible Growth Mechanism and the Supporting Evidence. *Nano Lett.* **2003**, *3*, 955−960.
(49) Luo, Q.; Feng, G.; Beller, M.; Jiao, H. Formic Acid Dehydrogenation on Ni(111) and Comparison with Pd(111) and Pt(111). *J. Phys. Chem. C* **2012**, *116*, 4149−4156.
(50) Zhou, S.; Qian, C.; Chen, X. Comparative Theoretical Study of Adsorption and Dehydrogenation of Formic Acid, Hydrazine and Isopropanol on Pd(111) Surface. *Catal. Lett.* **2011**, *141*, 726−734.
(51) Wang, Y.; Qi, Y.; Zhang, D.; Liu, C. New Insight into the Decomposition Mechanism of Formic Acid on Pd(111): Competing Formation of CO_2 and CO. *J. Phys. Chem. C* **2014**, *118*, 2067−2076.
(52) Prieto, P.; Nistor, V.; Nouneh, K.; Oyama, M.; Abd-Lefdil, M.; Díaz, R. XPS Study of Silver, Nickel and Nimetallic Silver−Nickel Nanoparticles Prepared by Seed-Mediated Growth. *Appl. Surf. Sci.* **2012**, *258*, 8807−8813.
(53) Fan, Z.; Zhang, H. Crystal Phase-Controlled Synthesis, Properties and Applications of Noble Metal Nanomaterials. *Chem. Soc. Rev.* **2016**, *45*, 63−82.

DOI: 10.1021/acsami.6b08091
ACS Appl. Mater. Interfaces 2016, 8, 20839−20848

(54) Fan, Z.; Luo, Z.; Huang, X.; Li, B.; Chen, Y.; Wang, J.; Hu, Y.; Zhang, H. Synthesis of 4H/fcc Noble Multimetallic Nanoribbons for Electrocatalytic Hydrogen Evolution Reaction. *J. Am. Chem. Soc.* **2016**, *138*, 1414−1419.
(55) Kusada, K.; Kobayashi, H.; Yamamoto, T.; Matsumura, S.; Sumi, N.; Sato, K.; Nagaoka, K.; Kubota, Y.; Kitagawa, H. Discovery of Face-Centered-Cubic Ruthenium Nanoparticles: Facile Size-Controlled Synthesis Using the Chemical Reduction Method. *J. Am. Chem. Soc.* **2013**, *135*, 5493−5496.
(56) Sun, Y. G.; Yin, Y. D.; Mayers, B. T.; Herricks, T.; Xia, Y. N. Uniform Silver Nanowires Synthesis by Reducing $AgNO_3$ with Ethylene Glycol in the Presence of Seeds and Poly(Vinyl Pyrrolidone). *Chem. Mater.* **2002**, *14*, 4736−4745.

DOI: 10.1021/acsami.6b08091
ACS Appl. Mater. Interfaces 2016, 8, 20839−20848